

Received December 22, 2021, accepted January 7, 2022, date of publication January 12, 2022, date of current version January 20, 2022.

Digital Object Identifier 10.1109/ACCESS.2022.3142529

Downlink Performance Analysis in MIMO UAV-Cellular Communication With LOS/NLOS Propagation Under 3D Beamforming

DINA ALKAMA¹, MOHAMED AMINE OUAMRI^{1,2}, MOHAMMED S. ALZAIDI³,
RABINDRA NATH SHAW⁴, (Senior Member, IEEE), MOHAMED AZNI¹,
AND SHERIF S. M. GHONEIM³, (Senior Member, IEEE)

¹Laboratoire d'informatique médicale (LIMED), Département ATE, Faculté de Technologie, Université de Bejaia, Bejaia 06000, Algeria

²Département de Télécommunication, Faculté de Génie Electrique et informatique, Université de Tizi Ouzou, Tizi Ouzou 15000, Algeria

³Electrical Engineering Department, College of Engineering, Taif University, Taif 21944, Saudi Arabia

⁴International Relations, Bharath Institute of Higher Education and Research, Chennai, Tamil Nadu 600073, India

Corresponding author: Mohamed Amine Ouamri (ouamrimouhamedamine@gmail.com)


This work was supported by the Taif University Researchers Supporting Project TURSP-2020/34, Taif university, Taif, Saudi Arabia.

ABSTRACT Integrating unmanned aerial vehicles (UAVs) as the base station is a recent progress and a promising solution to assist cellular networks to improve coverage. In this paper, an analytical framework is proposed to analyze coverage probability and capacity, using stochastic geometry. We incorporate the air-to-ground (A2G), and two-piece path loss model that undergoes millimeter wave (mmWave) channel fading in both line-of-site (LOS) and non-line-of-site (NLOS). Furthermore, we assume that all users' equipment's (UEs) are clustered around Terrestrial Base Stations (TBS) and UAVs, according to Poisson Cluster Process (PCP), i.e., Matern cluster process. We also propose Multiple-Input-Multiple-Output (MIMO) transmission where multiple single-antenna UAVs simultaneously communicate with TBS. Initially, we obtain expressions for association probability with each tier. After that, we derive downlink coverage expression based on signal-to-interference-plus-noise-ratio (SINR), by assuming 3D directional beamforming with UAV height being not fixed. Numerical results demonstrate the efficiency and accuracy of the proposed approach.

INDEX TERMS UAV communication, coverage analysis, MIMO, 3D beamforming, stochastic geometry, Nakagami-m fading.

I. INTRODUCTION

The use of unmanned aerial vehicles as base stations has emerged as a promising solution for providing coverage and capacity in fifth-generation (5G) cellular networks [1]. Due to their higher placement, unmanned aerial vehicles (UAV) have a greater chance to communicate with users on the ground, through line of light (LOS) links [2]. Moreover, UAV can assist terrestrial networks in preventing temporary congestion in ultra-dense places such as stadiums. With the significant increase in traffic demand, the millimeter wave (mmWave) has become an appealing choice for the 5G network. In particular, UAV equipped with a mmWave offers a considerable throughput at the same time.

The associate editor coordinating the review of this manuscript and approving it for publication was Jie Tang .

The coexistence of UAV base station and the terrestrial cellular network is widely studied. They face many challenges, including the behavior between air-to-ground (A2G) channel and terrestrial path loss and the UAV mobility impact [3]. In cellular communication that operate in mmWave frequency, the signals suffer from significant path loss (PL) and rain fade. This leads to a decrease in propagation distance [4]. Consequently, beamforming techniques can be used to transmit signals further into the 5G network. Indeed, beamforming concentrates the energy of the antenna array in the desired direction and increases the propagation distance [5]. Currently, 3 dimensional (3D) beamforming techniques are a more attractive and major challenge in future cellular networks. Such a system has significant benefits over previous approaches. Firstly, it provides links to increase the signal range by avoiding blockages [6]. Secondly, 3D beamforming allows a larger number of neighboring

streams to transmit simultaneously by reducing the interference range of beams [7]. Finally, it can connect any two racks with a single hop, limiting the need for multi-hop links.

UAV-assisted cellular networks' performance analysis has been a prominent topic, in particular coverage and capacity analysis [8], [9]. Without loss of generality, system-level analysis of a network is highly dependent on the deployment of the communicating entities such as base stations (BS) and user's equipment's (UEs). In recent works, stochastic geometry is introduced to model BS and UEs locations. For instance, authors in [10] considered a two-dimensional Poisson Point Process (PPP), in which UAVs are assumed to be located at the same height. In [11], UAV-assisted cellular network analysis is also investigated, where UEs are clustered around UAV according to Poisson Cluster Process (PCP). This representation is, according to 3rd Generation Partnership Project (3GPP), the most appropriate one, as in reality, UEs are more densely distributed in the areas where UAV-BS are deployed. Therefore, PCP can make available specific models for the location of UEs in UAV-assisted cellular networks. The anticipated potential of UAVs to provide better coverage has attracted significant research efforts to model and analyze the UAV-assisted cellular network's performance. Using tools from stochastic geometry, the coverage analysis for a single UAV was presented in [11], where UAVs were distributed according to 2D PPP. Recently, authors in [12] analyzed the downlink coverage probability of UAV assisted mmWave network, where user equipments (UEs) were clustered around the projections of UAVs. In addition to the coverage probability, the area spectral efficiency was determined. In [13], the performance of mobile UAV-UEs was studied under 3D practical antenna configurations. The impact of antenna elements on the coverage probability and handover rate of mobile UAV-UEs is incorporated. Moreover, [14] developed a 3D beamforming analytical model for wireless networks. In this study, different scenarios of 3D beamforming were compared in terms of throughput and coverage probability. PCP models have also been performed in the analysis of UAV-assisted cell networks in [15]. More specifically, the association probability and energy coverage of different tier UAVs and ground base stations (GBSs) are investigated in both line-of-site (LOS) and non-line-of-site (NLOS). It is worth noting that all of the aforementioned work considered a downlink transmission where the UAVs are placed at a constant height [2], [11], [15]. Similarly, in [16] the theoretical approach analysis of cellular-connected UAV by applying more practical 3D antenna radiation patterns was provided, but beamforming was not incorporated.

Motivated by the following rationale, this paper proposes an analytical framework to analyze the coverage and capacity of a UAV-assisted cellular network with a 3D beamforming technique via stochastic geometry and Nakagami- m fading. The main contribution of this document can be summarised as follows:

- We present a comprehensive and tractable analytical framework for analyzing UAV-assisted cellular communication, where a terrestrial base station (TBS) and UAV are distributed homogeneous PPP. We assume that all UAV are located at different heights compared to [3], [15] and equipped by Multiple-Input-Multiple-Output (MIMO). Moreover, 3D beamforming is incorporated into TBS to increase coverage.
- As opposed to [15], we derive the distances distribution and the associated probabilities of the UE, considering that path losses are different between tiers. In this proposed work, UEs are clustered around BSs according to PCP.
- We derive the analytical expressions for the coverage probability and capacity, taking into account the thermal noise in the general expression of SINR. Finally, Laplace transforms of interferences from each tier are computed to obtain the final expression.

The remainder of this paper is organized as follows. The system model introduced in Section II. Section III describes the UE association in both LOS and NLOS link. In Section IV, coverage and rate probability of the network is computed. In Section V, some numerical and simulation results are presented to further confirm the accuracy of the derived expressions, and conclusions are drawn in Section VI.

II. SYSTEM MODEL

A. NETWORK TOPOLOGY

A two-tier heterogeneous network (HetNet) consisting of TBSs and UAVs in investigated in the considered network. We assume that TBSs and UAVs are spatially distributed according to homogeneous PPP, denoted respectively by Φ_T and Φ_U , with respective densities $\lambda_T > 0$ and $\lambda_U > 0$. All signals are transmitted by TBSs and UAVs using the mmWave at constant powers P_T and P_U , respectively. UEs are clustered around BSs according to PCP, i.e., Matern cluster process denoted Φ_{UE} in a circular disc with a radius R_C [17]. As illustrated in Fig.1, it is assumed that N_i antennae equip the serving UAVs, and are located at different heights $H_z, z \in \{1, 2, \dots, Z\}$. Each UE associates with a single BS that provides the maximum received signal power.

B. CHANNEL MODEL

To analyze the network performance accurately, we adopt different path loss models to accommodate the differences between TBS-UE and UAV-UE communications. Link between BS and UE are mainly line-of-site (LOS) and non-line-of-site (NLOS).

For a given altitude H_z , the path loss model in the UAV scenario can be expressed as [18]:

$$PL_U^{LOS}(r_U) = \phi^{LOS}(r_U^2 + H_z^2)^{\frac{\alpha^{LOS}}{2}} \quad (1)$$

$$PL_U^{NLOS}(r_U) = \phi^{NLOS}(r_U^2 + H_z^2)^{\frac{\alpha^{NLOS}}{2}} \quad (2)$$

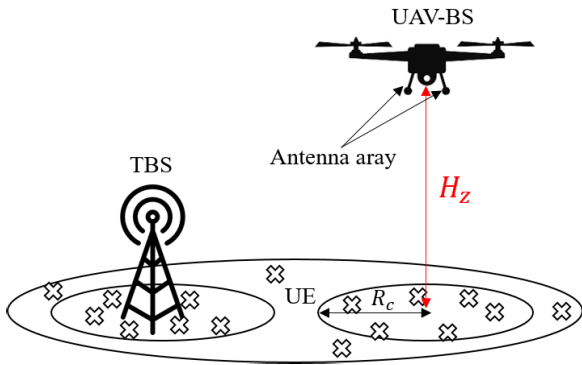


FIGURE 1. Network topology where transmitters are modeled as a HPPP.

where H_z is the altitude of the UAVs in meters, r is the distance between UE and the projection of UAV in the 2-D plane, φ^{LOS} and φ^{NLOS} are the additional path loss for LOS and NLOS links respectively. α^{LOS} and α^{NLOS} are the LOS and NLOS path loss exponents.

In the same way, the link between TBS and UEs is characterised by a propagation model. Given the distance r between the typical UE and TBS, the path loss model is given as follows [15]:

$$PL_T^k(r_T) = \begin{cases} PL^{LOS}(r_T) = A^{LOS} r_T^{-\alpha^{LOS}} \\ PL^{NLOS}(r_T) = A^{NLOS} r_T^{-\alpha^{NLOS}} \end{cases} \quad (3)$$

where A^{LOS} and A^{NLOS} represent the path losses at a reference distance of $r_T = 1km$.

C. SMALL-SCALE FADING

In cellular communication, small-scale fading is a characteristic of the short-term variation in the received signal amplitude resulting from constructive and destructive interference. Several statistical models exist to describe a general fading. It is assumed that each link follows independent Nakagami-m fading, with shape parameter given by $(N_L, 1/N_L)$ and $(N_N, 1/N_N)$ for LOS and NLOS links, respectively. In this paper, as in [15], [19], the power fading denoted h_k is a normalized Gamma random variable and its probability density function (PDF) is given by

$$f_h(x) = \frac{m^m}{\Gamma(m)} x^{m-1} e^{-mx} \quad x > 0 \quad (4)$$

where $\Gamma(m) = \int_0^\infty x^m e^{-x} dx$ is the Gamma function.

D. LINK STATE PROBABILITIES

To analyze the network performance accurately, we will assume the general approach of taking the LOS/NLOS links and their probabilities of occurrence separately. However, The LOS probability and NLOS probability depend on the nature of the environment, as well as the distance between UEs and the serving base station. When the communication is made between TBS and UE, the probability of having LOS is given as $\mathbb{P}_S^{LOS}(r) = e^{-\gamma r}$, where γ represents the blockage

parameter, which depends on the density and building parameters. On the other hand, the probability linking between a user and UAV in LOS is expressed as [11]

$$\mathbb{P}_U^{LOS}(r_U) = \frac{1}{1 + b \exp\left(-c \left(\frac{180}{\pi} \tan^{-1}\left(\frac{H_z}{r_U}\right) - b\right)\right)} \quad (5)$$

where b and c are constants that depend on the environment. The NLOS link probability is given by

$$\mathbb{P}_U^{NLOS}(r_U) = 1 - \mathbb{P}_{LOS}^{UAV}(r_U) \quad (6)$$

E. 3D BEAMFORMING

In this subsection, a 3D beamforming approach that leverages ceiling reflections to connect racks wirelessly is proposed. Indeed, 3D beamforming avoids obstacles in the horizontal plane, thus eliminating the problem of antenna blockage. As illustrated in Fig.2, the vertical gain of the BS antenna radiation pattern in the direction of the UE is expressed as [20]

$$w(\beta_j, \theta_i^j) = 10^{-0.1 \times \min\left[12 \left(\frac{\theta_i^j - \beta_j}{\theta_{3dB}}\right)^2, SLL\right]} \quad (7)$$

where β_j is the tilt angle of the BS antenna pattern and θ_i^j is the vertical UE angle of arrival. Also θ_{3dB} and SLL are the half-power beamwidth (HPBW) and the side lobe level of the BS antenna pattern in the vertical domain, respectively.

III. ASSOCIATION PROBABILITIES

A cell association criterion based on the strongest long-term averaged maximum received power is assumed [21]. Furthermore, we consider that the LOS/NLOS transmission between TBS and UE is independent of the LOS/NLOS between UAV to UE link. In our approach, the association probability depends on the distance distribution separating UE to the serving BS. Under this assumption, the distribution of the distance of a typical user from its serving BS is given by lemma 1. The received power from UAV and TBS, transmitting with a power level P_T and P_U respectively is expressed by

$$P_r^U = P_U G_U w_U(\beta_j, \theta_i^j) PL_U^k(r_U)^{-1} \quad (8)$$

$$P_r^T = P_T G_T w_T(\beta_j, \theta_i^j) PL_T^k(r_T)^{-1} \quad (9)$$

where $G_U = N_t - N_{UE} + 1$ is the array gain for zero forcing beamforming transmission [22]. UAV transmit simultaneously to N_{UE} users such that $N_t \gg N_{UE}$.

Lemma 1: The Complimentary Cumulative Distribution Function (CCDF) and PDF of the nearest distance from the typical UE to a LOS/NLOS BS can be expressed as follows

From UAV-to-UE

$$CCDF : F_{r_U}^k(y) = W_U^{k-1} \int_l^R \mathbb{P}_U^k\left(\sqrt{D^2 + H_z^2}\right) f_D(d) dd \quad (10)$$

$$k \in \{LOS, NLOS\} \text{ and } l = \sqrt{y^2 - H_z^2}$$

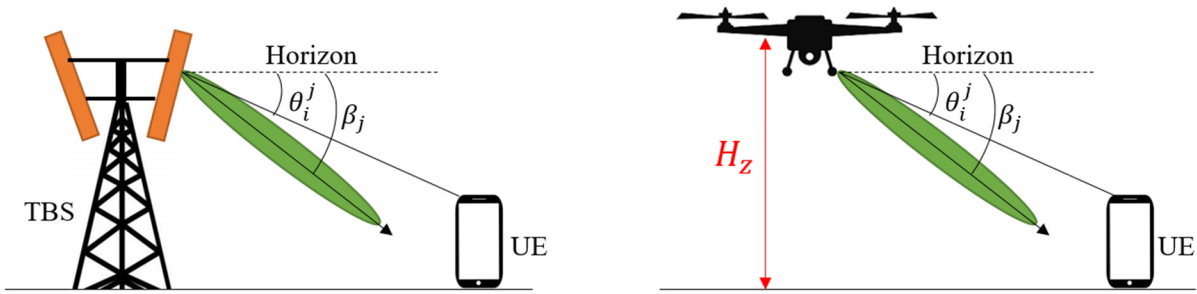


FIGURE 2. 3D beamforming in both TBS and UAV.

$$PDF : f_{r_U^k}(y) = \frac{2y \mathbb{P}_U^k(y)}{R^2} W_U^{k-1} \quad (11)$$

From TBS-to-UE

$$CCDF : F_{r_T^k}(y) = \exp - \frac{R^2 - y^2}{R^2 W_S^k} \quad (12)$$

$$PDF : f_{r_T^k}(y) = \frac{2y}{R^2 W_S^k} \quad (13)$$

where $W_S^k = 1 - e^{-2\pi\lambda_S \int_0^y t \mathbb{P}_S^k(t) dt}$, $W_U^k = 1 - e^{-2\pi\lambda_U \int_{H_z}^\infty t \mathbb{P}_U^k(t) dt}$ are the probability that the typical UE has at least one LOS/NLOS TBS and UAV respectively [23].

Proof:

$$\begin{aligned} F_{r_U} &= \mathbb{P}(r > x) \\ &= W_U^{k-1} E_D [(\mathbb{P}(r > x) | k, D) \mathbb{P}(k | D)] \\ &= W_U^{k-1} E_D \left[(\mathbb{P}(\sqrt{D^2 + H_z^2} > x | k, D) \mathbb{P}_U^k(\sqrt{D^2 + H_z^2}) \right] \\ &= W_U^{k-1} E_D \left[\mathbb{P}\left(D > \sqrt{x^2 - H_z^2}\right) \mathbb{P}_U^k\left(\sqrt{D^2 + H_z^2}\right) \right] \\ &= W_U^{k-1} \int_l^\infty \mathbb{P}_U^k\left(\sqrt{D^2 + H_z^2}\right) f_D(d) dd \quad (14) \end{aligned}$$

where $f_D(d) = \left(1 - \frac{d^2}{r_U^2}\right) \mathbb{1}(0 \leq x \leq R)$ is the distribution of distance from UE to its UAV projection (cluster center). Then, we derive the association probability of an arbitrary UE with BS in both LOS/NLOS conditions.

Lemma 2: The probability that atypical user is associated with the nearest UAV/TBS in LOS/NLOS condition can be given in (15) and (16), as shown at the bottom of the next page.

Proof: see appendix A

IV. PERFORMANCE ANALYSIS

Under the system model defined earlier, we evaluate the network performance from a coverage and rate perspective. The major results is a general expression for the coverage and

rate probability. For a given SINR threshold τ , the coverage and rate probabilities at the typical user are expressed as

$$\mathcal{P}_{cov} = \mathbb{P}(SINR > \tau) \quad (17)$$

$$\mathcal{R} = \mathbb{E}[\ln(1 + SINR)] \quad (18)$$

A. SINR EXPRESSION

Our model considers that the link between the UE and its associated BS (UAV, TBS) is interfered by all other adjacent BS. When the user is associated with TBS, total interference combines the interference coming from NLOS UAV and all TBS. Oppositely, in the UAV-UE communication case, the aggregate interference is the sum of two elements as the interference received from LOS/NLOS UAV and LOS/NLOS TBS. The intratier interference can thus be given as follows:

$$I = \begin{cases} I_{U'}^{NLOS} + I_T^k & \text{if UE is associated with UAV} \\ I_{T'}^b + I_U^k & \text{if UE is associated with TBS} \end{cases} \quad (19)$$

where

$$I_{U'}^{NLOS} = \sum_{\substack{U' \neq U, \\ U' \in \Phi_U}} P_{U'} G_{U'} h_{U'} w_{U'} (\beta_j, \theta_i^j) PL_{U'}^{NLOS}(r_{U'})^{-1} \quad (20)$$

$$I_T^k = \sum_{T \in \Phi_T} P_T G_T h_T w_T (\beta_j, \theta_i^j) PL_T^k(r_T)^{-1} \quad (21)$$

$$I_{T'}^b = \sum_{T' \neq T, T' \in \Phi_T} P_{T'} G_{T'} h_{T'} w_{T'} (\beta_j, \theta_i^j) PL_{T'}^b(r_{T'})^{-1} \quad (22)$$

$$I_U^k = \sum_{U \in \Phi_U} P_U G_U h_U w_U (\beta_j, \theta_i^j) PL_U^k(r_U)^{-1} \quad (23)$$

The downlink SINR for the typical user can be expressed as:

$$SINR_U = \frac{P_U G_U h_U w_U (\beta_j, \theta_i^j) PL_U^k(r_{U_0})^{-1}}{I + \sigma^2} \quad (24)$$

$$SINR_T = \frac{P_T G_T h_T w_T (\beta_j, \theta_i^j) PL_T^k(r_{T_0})^{-1}}{I + \sigma^2} \quad (25)$$

where σ^2 is the noise power. r_{U_0} and r_{T_0} are the distances from the typical UE_0 to its serving UAV, TBS respectively.

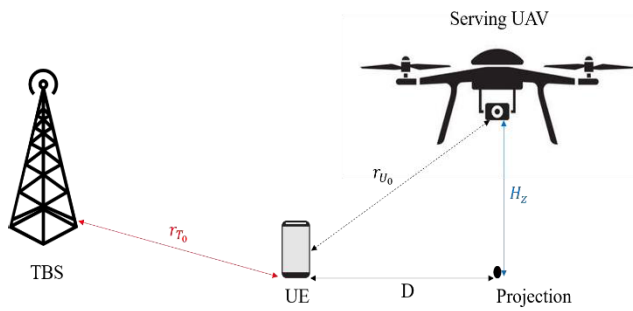


FIGURE 3. Distance from serving BS and UE.

B. COVERAGE PROBABILITY

In the following, we use the distance distributions and the SINR expression to evaluate the coverage probability. This analysis reflects the probability that a given BS serves a typical user. We evaluate the total coverage probability of the proposed model which is mathematically expressed as

$$\mathcal{P}_c^{Tot} = \mathcal{A}_U^k \mathcal{P}_{cov}^U + \mathcal{A}_T^k \mathcal{P}_{cov}^T \tag{26}$$

where \mathcal{A}_U^k and \mathcal{A}_T^k are association probabilities as given in the previous section. \mathcal{P}_{cov}^U and \mathcal{P}_{cov}^T are conditional coverage probabilities whose final result is given in Theorem 1. To approximate the conditional coverage probability expression, we apply a tight limit to the Cumulative Distribution Function (CDF) of the Gamma distribution [22].

Theorem 1: If UE is served by LOS/NLOS link, the conditional coverage probability can be expressed as

$$\mathcal{P}_{c,k}^U = \sum_{n=1}^{N_k} (-1)^{n+1} \binom{N_k}{n} \mathbb{E}_{r_{U_0}} \left[\mathcal{L}_O(-\beta^k \mu) \right] \tag{27}$$

where $\mu = \frac{\tau PL_U^k(r_{U_0})}{P_U G_U w_U(\beta_j, \theta_i^j)}$ and $\mathcal{L}_O(-\beta^k \mu) = \exp(-\sigma^2 \mu) \times (\mathcal{L}_{I_U^{NLOS}} + \mathcal{L}_{I_T^k})$ are the Laplace transform of different interference indicated above and given by (28), (29), as shown at the bottom of the page. Thus, when TBS serves the UE, the conditional coverage probability can be expressed as:

$$\mathcal{P}_{c,k}^T = \mathbb{E}_{G_T} \left[\sum_{n=1}^{N_k} (-1)^{n+1} \binom{N_k}{n} e^{n\varepsilon \sigma^2} \mathcal{L}_I(n\varepsilon) \right] \tag{30}$$

where $\varepsilon = \frac{\beta^k \tau PL_T^k(r_{T_0})}{P_T G_T w_T(\beta_j, \theta_i^j)}$ and $\beta^k = (N_k!)^{-\frac{1}{N_k}}$. Note that $\mathcal{L}_I(n\varepsilon) = \mathcal{L}_{I_T^k} + \mathcal{L}_{I_U^{NLOS}}$ and given by (31), (32), as shown at the bottom of the next page.

C. RATE PROBABILITY

After calculating the probability of coverage in both cases, i.e., UAV and TBS, the average achievable rate is computed using the Shannon capacity formula. It is useful to analyze this metric because the achievable rates provide a better assessment of the system’s spectrum efficiency. It should be noted that the average achievable rate reported here is in the unit of Mbits. Hence, theorem 2, gives the average achievable rate for a typical UE.

Theorem 2: The average achievable R rate of UE when using 3D beamforming can be expressed as

$$\mathcal{R}_U^k = \int_{v>0} \mathbb{E}_{r_{U_0}, \Theta} \left[\frac{\Gamma_u \left(m, m \frac{PL_U^k(r_{U_0})}{P_U G_U w_U(\beta_j, \theta_i^j)} \right)}{\Gamma(m) \Theta} \times (e^v - 1) \Theta \right] dv \tag{33}$$

$$\mathcal{R}_T^k = \int_{v>0} \mathbb{E}_{r_{T_0}, \Theta} \left[\frac{\Gamma_u \left(m, m \frac{PL_T^k(r_{T_0})}{P_T G_T w_T(\beta_j, \theta_i^j)} \right)}{\Gamma(m) \Theta} \times (e^v - 1) \Theta \right] dv \tag{34}$$

$$\mathcal{A}_U^k = \int_{H_z}^{\infty} \exp \left(-\pi \lambda_T \left(\frac{P_T G_T w_T(\beta_j, \theta_i^j) \varphi^k}{P_U G_U w_U(\beta_j, \theta_i^j) A^k} (r_U^2 + H_z^2)^{\frac{\alpha_U^k}{2}} \right)^{\frac{1}{\alpha_T^k}} \right) \times \frac{2y \mathbb{P}_U^k(r_U)}{R^2} W_U^{k-1} dr_U \tag{15}$$

$$\mathcal{A}_T^k = \int_0^{\infty} \exp \left(-2\pi \lambda_U \int_{H_z}^{\sqrt{Q}} \mathbb{P}_U^k(r_U) r_U dr_U \right) \times \frac{2r_T}{R^2} W_S^{k-1} dr_T \tag{16}$$

$$\mathcal{L}_{I_U^{NLOS}}(\mu) = \exp \left(-2\pi \lambda_U \mathbb{E}_{G_U} \left[\left(\int_x^{\infty} 1 - \left(\frac{1}{1 + \frac{\mu P_{U'} G_{U'} w_{U'}(\beta_j, \theta_i^j) \varphi^b (r_T^2 + H_z^2)^{\frac{\alpha_b}{2}}}{N_k}} \right) \right)^{NLOS} r \mathbb{P}_{U'}^{NLOS}(r) dr \right] \right) \tag{28}$$

$$\mathcal{L}_{I_T}(\varepsilon) = \exp \left(-2\pi \lambda_T \mathbb{E}_{G_T} \left[\left(\int_x^{\infty} 1 - \left(\frac{1}{1 + \frac{\varepsilon P_T G_T w_T(\beta_j, \theta_i^j) A^k r^{-\alpha^k}}{N_k}} \right)^{N_k} \right) r \mathbb{P}_T^k(r) dr \right] \right) \tag{29}$$

where $\Gamma_u \left(m, m \frac{PL_U^k(r_{U_0})}{P_U G_U w_U (\beta_j, \theta_i^j)} \right) / \Gamma(m)$ is the complementary cumulative distribution function (CCDF) of the gamma distribution [23].

Proof:

$$\mathcal{R}_U^k = \mathbb{E} [\ln(1 + SINR)] = \int_{v>0} \mathbb{P}(\ln(1 + SINR) > v) dv \quad (35)$$

The method of computing Laplace transform \mathcal{L}_I can be found in [26].

By using $\mathbb{E}[X] = \int_{v>0} \mathbb{P}(x > v) dv$ for a positive random variable [27], we obtain:

$$\begin{aligned} \mathcal{R}_U^k &> \mathbb{P} \left(\ln \left(1 + \frac{P_U G_U h_U w_U (\beta_j, \theta_i^j)}{(I + \sigma^2) PL_U^k(r_{U_0})} \right) \right) > v dv \\ \mathcal{R}_U^k &= \int_{v>0} \\ &\times \mathbb{E}_{r_{U_0}, O} \left[\mathbb{P} \left(h_U > \frac{v PL_U^k(r_{U_0})}{P_U G_U w_U (\beta_j, \theta_i^j)} (I + \sigma^2) \right) \right] dv \\ \mathcal{R}_U^k &= \int_{v>0} \mathbb{E}_{r_{U_0}, O} \left[\frac{\Gamma_u \left(m, m \frac{PL_U^k(r_{U_0})}{P_U G_U w_U (\beta_j, \theta_i^j)} \right)}{\Gamma(m)} \right] dv \quad (36) \end{aligned}$$

The same calculation is applied to obtain the rate probability for TBS.

V. NUMERICAL AND SIMULATION RESULTS

This section evaluates the proposed analytical modeling versus the simulations results for coverage and rate probabilities. The theoretical expressions obtained are validated using Monte Carlo. In the simulation, we assume that the transmit power of TBSs and UAVs are 30 dBm and 24 dBm respectively. We include 3D beamforming to demonstrate the advantage in improving coverage. The parameters values are listed in Table 1.

First, we examine the effect of 3D beamforming on the association probability while varying the height of the deployed UAVs. As shown in Fig.4, 3D beamforming significantly improves the association probability. Indeed, from a

TABLE 1. System parameters.

Parameter	Value
λ_S, λ_U	$10^{-2}/m^2 \quad 10^{-3}/m^2$
Noise power σ^2	1, -174 dBm/Hz
Carrier frequency f	28 GHz
$\alpha^{LOS}, \alpha^{NLOS}, \varphi^{LOS}, \varphi^{NLOS}$	2,3,1,1
SINR threshold τ	-90dBm

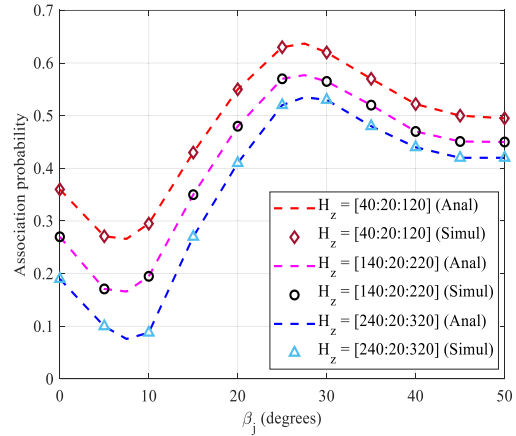


FIGURE 4. Association probability as function of antenna down tilt with different values of UAV height H_z variation.

certain tilt value (at about 8 degrees), the association probability increases and then becomes stable. It is because UAV and TBS can direct their beam toward the user through a larger down tilt. Furthermore, when the height varies between 40 meters and 120 meters, the total association probability increases. This can be explained from the fact that when the height of the UAVs varies between 40 and 120 meters, the probability of the link in LOS increases, i.e. the blocking phenomenon becomes less important. Fig.4 also demonstrates that there is an optimal down tilt for each UAV height value in which the association probability is maximized.

Regarding the impact of the cluster size on association probability in the case where we apply a 3D beamforming and directional beamforming respectively, Fig.5 shows that as the cluster size of UAVs increases, the probability of association with UAVs decreases whereas the probability of association with TBS increases. The displacement of UEs can explain this to adjacent TBS clusters. We also observe that the 3D beamforming improves the association probability when the cluster size increases, compared to the

$$\mathcal{L}_{I_U^{NLOS}}(\mu) = \exp \left(-2\pi \lambda_U \mathbb{E}_{G_U} \left[\left(\int_x^\infty 1 - \left(\frac{1}{1 + \frac{\mu P_U G_U w_U (\beta_j, \theta_i^j) \phi^b (r_T^2 + H_z^2)^{\frac{a^b}{2}}}{N_k}} \right)^{N_k} \right) r \mathbb{P}_U^{NLOS}(r) dr \right] \right) \quad (31)$$

$$\mathcal{L}_{I_{T'}}(\varepsilon) = \exp \left(-2\pi \lambda_T \mathbb{E}_{G_{T'}} \left[\left(\int_x^\infty 1 - \left(\frac{1}{1 + \frac{\varepsilon P_{T'} G_{T'} w_{T'} (\beta_j, \theta_i^j) A^k r^{-a^k}}{N_k}} \right)^{N_k} \right) r \mathbb{P}_{T'}^k(r) dr \right] \right) \quad (32)$$

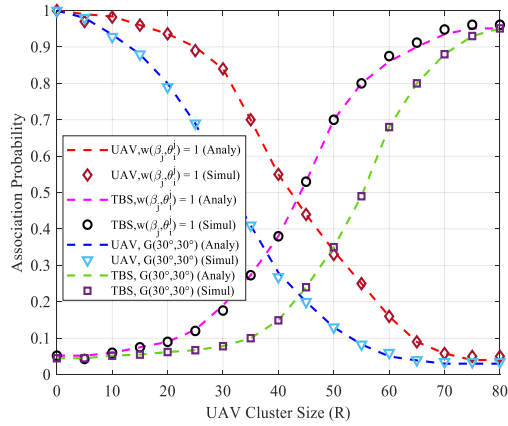


FIGURE 5. Association probability versus UAV cluster size with different beamforming (3D beamforming and directional beamforming).

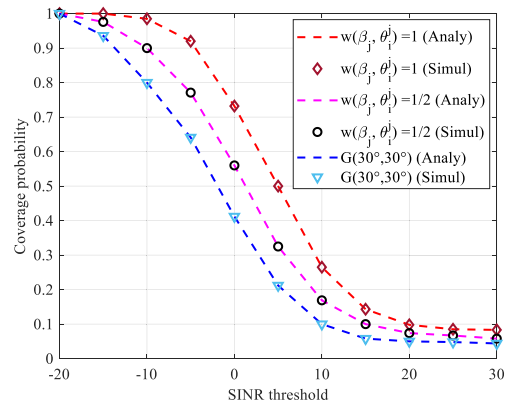


FIGURE 6. Coverage probability comparison as function of SINR threshold: 3D beamforming vs. directional beamforming.

directional beamforming. Thus, the application of 3D beamforming increases the possibility of having LOS connections despite the increase in cluster size.

In Fig.6 and Fig.7, we study the influence of 3D beamforming and UAV height on coverage probability. From Fig.6, it can be observed that the coverage performance in terms of SINR with 3D beamforming is greater than with 2D beamforming. This is expected, as the interference level degrades with increasing the vertical gain of the BS antenna radiation pattern $w(\beta_j, \theta_j^i)$. More specifically, in Fig.7, when UAVs' altitudes increase, the coverage probability degrades. In addition, the path loss exponent has a significant impact on the coverage probability. Indeed, a large increase in value leads to a decrease in coverage probability. The illustration also reveals the need for a correlation between the height of the UAVs and the path loss exponent to achieve satisfactory coverage.

Next, we compare the coverage probability for different values of the number of antennas used in the transmission. Fig.8 illustrates the relationship between the UAVs height and the number of antennas applied. It can be seen that increasing the number of antennas leads to an improvement in coverage probability, despite the increasing of UAVs height.

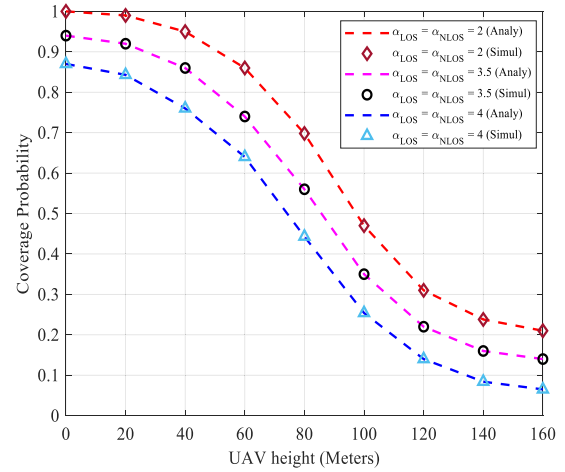


FIGURE 7. Coverage probability as function of UAV height with different path loss exponent.

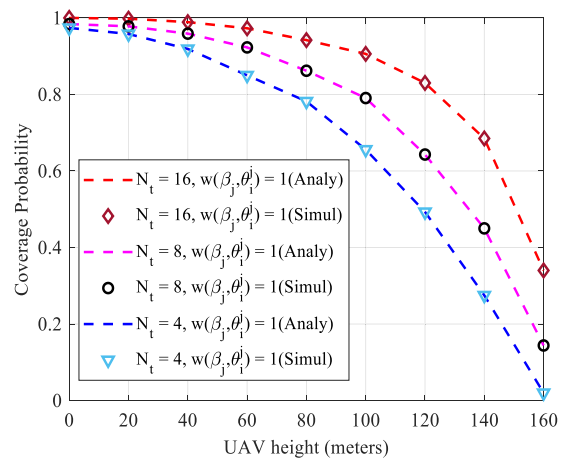


FIGURE 8. Coverage probability as function of UAV height with different number of antenna.

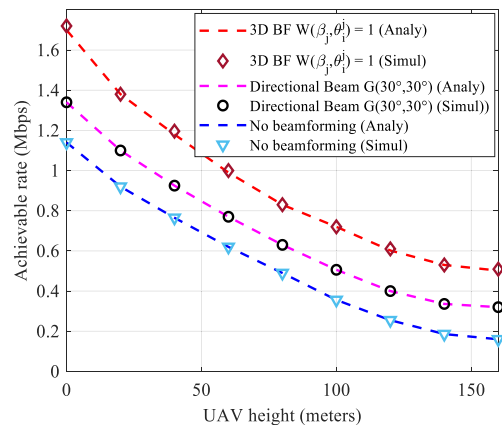


FIGURE 9. Achievable rate as function of UAV height with different beamforming model.

Thus, under such analysis, the optimum number of antennas can be determined using this model. In Fig.9, we plot the variation of rate probability as a function of UAVs height for

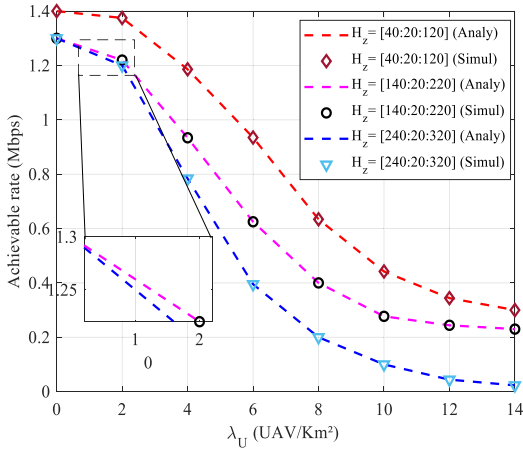


FIGURE 10. Achievable rate as function of UAV density with different UAV height and 3D beamforming.

different beamforming techniques. From this figure, we conclude that as the height of the UAVs increases the achievable rate decreases. This is caused by the influence of the increased interference power from adjacent BS on the communication. We can also observe that the 3D beamforming model has a better performance compared to directional beamforming. Therefore, 3D beamforming is more robust to intercell interference.

Finally, Fig.10 depicts the impact of the UAVs density on the average rate probability. We note that as UAVs density λ_U increase, the achievable rate decreases for different values of UAV height variation. Indeed, this this degradation is mainly due to the increase of overlapping areas between clusters, resulting in strong inter-cell interference on the typical user.

VI. CONCLUSION

In this paper, we have studied MIMO-UAV-assisted cellular networks' performance under 3D beamforming and Nakagami-m fading. Different network parameters are taken into account, such as down tilt, UAV height, and number of antennas in transmission. In our model, the UEs locations are clustered around the base station using Poisson Cluster Process, i.e., Matern Cluster Process. Considering LOS and NLOS conditions, we derived the downlink coverage probabilities and rates by applying stochastic geometry laws. A comparison between the 3D beamforming and directional beam was investigated which has shown greater efficiency with 3D beamforming. We can also conclude that the user's equipment are more likely to be associated with UAV when the altitude is low. Interestingly, when UAVs are located at different heights, the coverage probability was better illustrated.

In future work, we propose to analyse the coverage and handover probability for UAV assisted mmWave network considering that the mobility of the UAVs is realized along an orbital path.

APPENDIX

A. PROOF OF ASSOCIATION PROBABILITY

1) The UAV association probability.

$$\begin{aligned} \mathcal{A}_U^k &= \mathbb{E}_{r_U} [\mathbb{P} (P_r^U (r_U) > P_r^T (r_T))] \\ \mathcal{A}_U^k &= \mathbb{E}_{r_U} \left[\mathbb{P} \left(P_U G_U W_U (\beta_j, \theta_i^j) PL_U^k (r_U)^{-1} \right. \right. \\ &\quad \left. \left. > P_T G_T W_T (\beta_j, \theta_i^j) PL_T^k (r_T)^{-1} \right) \right] \\ \mathcal{A}_U^k &= \mathbb{E}_{r_U} \left[\mathbb{P} \left(PL_T^k (r_T) > \frac{P_T G_T W_T (\beta_j, \theta_i^j)}{P_U G_U W_U (\beta_j, \theta_i^j)} \right. \right. \\ &\quad \left. \left. \times \varphi^k \left(r_U^2 + H_z^2 \right)^{\frac{\alpha_U^k}{2}} \right) \right] \\ \mathcal{A}_U^k &= \int_{H_z}^{\infty} \left[\mathbb{P} \left(r_T > \left(\frac{P_T G_T W_T (\beta_j, \theta_i^j) \varphi^k}{P_U G_U W_U (\beta_j, \theta_i^j) A^k} \right. \right. \right. \\ &\quad \left. \left. \times \left(r_U^2 + H_z^2 \right)^{\frac{\alpha_U^k}{2}} \right)^{\frac{1}{\alpha_T^k}} \right) \times f_{r_U}^k (r_U) \right] dr_U \quad (37) \end{aligned}$$

By apply the null probability of a 2-D poisson process

$$\begin{aligned} \mathbb{P} \left(r_T > \left(\frac{P_T G_T W_T (\beta_j, \theta_i^j) \varphi^k}{P_U G_U W_U (\beta_j, \theta_i^j) A^k} \right) \left(r_U^2 + H_z^2 \right)^{\frac{\alpha_U^k}{2}} \right)^{\frac{1}{\alpha_T^k}} \right) \text{ is given} \\ \text{by:} \\ \exp \left(-\pi \lambda_T \left(\frac{P_T G_T W_T (\beta_j, \theta_i^j) \varphi^k}{P_U G_U W_U (\beta_j, \theta_i^j) A^k} \right) \left(r_U^2 + H_z^2 \right)^{\frac{\alpha_U^k}{2}} \right)^{\frac{1}{\alpha_T^k}} \right) \quad (38) \end{aligned}$$

Substituting (38) and (11) into (37), we obtain the result in (15).

2) The TBS association probability.

$$\begin{aligned} \mathcal{A}_T^k &= \mathbb{E}_{r_T} [\mathbb{P} (P_r^T (r_T) > P_r^U (r_U))] \\ \mathcal{A}_T^k &= \mathbb{E}_{r_T} \left[\mathbb{P} \left(P_T G_T W_T (\beta_j, \theta_i^j) PL_T^k (r_T)^{-1} \right. \right. \\ &\quad \left. \left. > P_U G_U W_U (\beta_j, \theta_i^j) PL_U^k (r_U)^{-1} \right) \right] \\ \mathcal{A}_T^k &= \mathbb{E}_{r_T} \left[\mathbb{P} \left(\left(r_U^2 + H_z^2 \right)^{\frac{\alpha_U^k}{2}} \right. \right. \\ &\quad \left. \left. > \frac{P_U G_U W_U (\beta_j, \theta_i^j) A^k \alpha_T^k}{P_T G_T W_T (\beta_j, \theta_i^j) \varphi^k} r_T \right) \right] \\ \mathcal{A}_T^k &= \int_0^{\infty} \left[\mathbb{P} \left(r_U > \sqrt{\left(\frac{P_U G_U W_U (\beta_j, \theta_i^j) A^k \alpha_T^k}{P_T G_T W_T (\beta_j, \theta_i^j) \varphi^k} r_T \right)^{\frac{2}{\alpha_U^k}} - H_z^2} \right) \right. \\ &\quad \left. \times f_{r_T}^k (r_T) \right] \times dr_T \quad (39) \end{aligned}$$

By apply the null probability of a 2-D poisson process

$$\mathbb{P} \left(r_U > \sqrt{\left(\frac{P_U G_U W_U (\beta_j, \theta_i^j)^{A^k} r_T^{\alpha_U^k}}{P_T G_T W_T (\beta_j, \theta_i^j)^{\phi^k}} \right)^{\frac{2}{\alpha_U^k}} - H_z^2} \right) \text{ is given by:}$$

$$\exp \left(-2\pi \lambda_U \int_{H_z}^{\sqrt{Q}} \mathbb{P}_U^k(r_U) r_U dr_U \right) \quad (40)$$

$$\text{where } Q = \sqrt{\left(\frac{P_U G_U W_U (\beta_j, \theta_i^j)^{A^k} r_T^{\alpha_U^k}}{P_T G_T W_T (\beta_j, \theta_i^j)^{\phi^k}} \right)^{\frac{2}{\alpha_U^k}} - H_z^2}.$$

Substituting (40) and (13) into (39), we obtain the result in (16).

B. PROOF OF COVERAGE PROBABILITY

1) The UAV coverage probability

$$\begin{aligned} \mathcal{P}_{c,k}^U &= \mathbb{P}[SINR_U > \tau] \\ &= \mathbb{P} \left[\frac{P_U G_U h_U W_U (\beta_j, \theta_i^j) PL_U^k (r_{U_0})^{-1}}{I + \sigma^2} > \tau \right] \\ &\times \mathbb{P} \left[h_U > \frac{\tau}{P_U G_U W_U (\beta_j, \theta_i^j) PL_U^k (r_{U_0})^{-1}} \right. \\ &\left. \times (I_{U'}^{NLOS} + I_T^k + \sigma^2) \right] \\ &= \mathbb{E}_{r_{U_0}} \left[\mathbb{P} \left(h_U > \frac{\tau}{P_U G_U W_U (\beta_j, \theta_i^j) PL_U^k (r_{U_0})^{-1}} \circ \right) \right] \\ &= \mathbb{E}_{r_{U_0}} \left[1 - \mathbb{E}_O \left[\left(1 - e^{-\frac{\tau PL_U^k (r_{U_0})}{P_U G_U W_U (\beta_j, \theta_i^j) \circ}} \right)^{N_k} \right] \right] \end{aligned}$$

where (26) is to from the definition of the binomial theorem. By bounding the gamma distribution as [Theorem1, 24]

$$(1 - e^{\beta_1 m})^m < \frac{\Gamma_u(m)}{\Gamma(m)} < (1 - e^{\beta_2 m})^m$$

where $\Gamma_u(m) = \int_m^\infty t^{m-1} e^{-t} dt$ is the incomplete gamma function [25]

$$\begin{aligned} &= \mathbb{E}_{r_{U_0}, \circ} \left[\sum_{n=1}^{N_k} (-1)^{n+1} \binom{N_k}{n} \exp(-\beta^k \mu \circ) \right] \\ &= \sum_{n=1}^{N_k} (-1)^{n+1} \binom{N_k}{n} \mathbb{E}_{r_{U_0}} \left[\mathcal{L}_O(-\beta^k \mu) \right] \quad (41) \end{aligned}$$

where $\mu = \frac{\tau PL_U^k (r_{U_0})}{P_U G_U W_U (\beta_j, \theta_i^j)}$, $\circ = I_{U'}^{NLOS} + I_T^k$ and $\mathcal{L}_O(-\beta^k \mu) = \exp(\sigma^2 \mu) \mathcal{L}_{I_{U'}^{NLOS}} \mathcal{L}_{I_T^k}$ are the Laplace

transform of different interference indicated above and given by lemma 2

2) The TBS coverage probability

$$\begin{aligned} \mathcal{P}_{c,k}^U &= \mathbb{P}[SINR_U > \tau] \\ &= \mathbb{P} \left[\frac{\mathbb{P}_T G_T h_T W_T (\beta_j, \theta_i^j) PL_T^k (r_{T_0})^{-1}}{I + \sigma^2} > \tau \right] \\ &= \mathbb{P} \left[h_T > \frac{\tau PL_T^k (r_{T_0})}{P_T G_T W_T (\beta_j, \theta_i^j)} (T + \sigma^2) \right] \\ &= \mathbb{E}_{G_T} \left[1 - \mathbb{E}_I \left[\left(1 - e^{-\frac{\tau PL_T^k (r_{T_0})}{P_T G_T W_T (\beta_j, \theta_i^j)} (T + \sigma^2)} \right)^{N_k} \right] \right] \\ &= \mathbb{E}_{G_T} \left[\sum_{n=1}^{N_k} (-1)^{n+1} \binom{N_k}{n} \mathbb{E}_I \left[e^{-n\epsilon (I + \sigma^2)} \right] \right] \\ &= \mathbb{E}_{G_T} \left[\sum_{n=1}^{N_k} (-1)^{n+1} \binom{N_k}{n} \mathbb{E}_I \left[e^{-n\epsilon I} \right] e^{-n\sigma^2} \right] \\ &= \mathbb{E}_{G_T} \left[\sum_{n=1}^{N_k} (-1)^{n+1} \binom{N_k}{n} e^{-n\epsilon \sigma^2} \mathcal{L}_{I_T^k} + \mathcal{L}_{I_U^{NLOS}} \right] \\ \mathcal{P}_{c,k}^T &= \mathbb{E}_{G_T} \left[\sum_{n=1}^{N_k} (-1)^{n+1} \binom{N_k}{n} e^{n\epsilon \sigma^2} \mathcal{L}_I(n\epsilon) \right] \end{aligned}$$

ACKNOWLEDGMENT

The authors would like to acknowledge the financial support received from Taif University Researchers Supporting Project Number TURSP-2020/34, Taif University, Taif, Saudi Arabia.

REFERENCES

- [1] A. A. Khuwaja, G. Zheng, Y. Chen, and W. Feng, "Optimum deployment of multiple UAVs for coverage area maximization in the presence of co-channel interference," *IEEE Access*, vol. 7, pp. 85203–85212, 2019.
- [2] X. Xu and Y. Zeng, "Cellular-connected UAV: Performance analysis with 3D antenna modelling," in *Proc. IEEE Int. Conf. Commun. Workshops (ICC Workshops)*, May 2019, pp. 1–6.
- [3] C. Fan, T. Zhang, and Z. Zeng, "Coverage and rate analysis of cache-enabled vertical heterogeneous networks," *IEEE Access*, vol. 7, pp. 153519–153532, 2019.
- [4] M. A. Ouamri, M.-E. Oteşteanu, A. Isar, and M. Azni, "Coverage, handoff and cost optimization for 5G heterogeneous network," *Phys. Commun.*, vol. 39, Apr. 2020, Art. no. 101037.
- [5] X. Yu, J. Zhang, M. Haenggi, and K. B. Letaief, "Coverage analysis for millimeter wave networks: The impact of directional antenna arrays," *IEEE J. Sel. Areas Commun.*, vol. 35, no. 7, pp. 1498–1512, Jul. 2017.
- [6] L. Zhu, J. Zhang, Z. Xiao, X. Cao, D. O. Wu, and X.-G. Xia, "3-D beamforming for flexible coverage in millimeter-wave UAV communications," *IEEE Wireless Commun. Lett.*, vol. 8, no. 3, pp. 837–840, Jun. 2019.
- [7] H. Lu, Y. Zeng, S. Jin, and R. Zhang, "Aerial intelligent reflecting surface: Joint placement and passive beamforming design with 3D beam flattening," *IEEE Trans. Wireless Commun.*, vol. 20, no. 7, pp. 4128–4143, Jul. 2021.
- [8] K. K. Armeniakos, P. S. Bithas, and A. G. Kanatas, "SIR analysis in 3D UAV networks: A stochastic geometry approach," *IEEE Access*, vol. 8, pp. 204963–204973, 2020.
- [9] D. Kim, J. Lee, and T. Q. S. Quek, "Multi-layer unmanned aerial vehicle networks: Modeling and performance analysis," *IEEE Trans. Wireless Commun.*, vol. 19, no. 1, pp. 325–339, Jan. 2020.

- [10] B. Galkin, J. Kibilda, and L. A. DaSilva, "Coverage analysis for low-altitude UAV networks in urban environments," in *Proc. IEEE Global Commun. Conf. (GLOBECOM)*, Dec. 2017, pp. 1–6.
- [11] E. Turgut and M. C. Gursoy, "Downlink analysis in unmanned aerial vehicle (UAV) assisted cellular networks with clustered users," *IEEE Access*, vol. 6, pp. 36313–36324, 2018.
- [12] M. Mozaffari, W. Saad, M. Bennis, and M. Debbah, "Unmanned aerial vehicle with underlaid device-to-device communications: Performance and tradeoffs," *IEEE Trans. Wireless Commun.*, vol. 15, no. 6, pp. 3949–3963, Jun. 2016.
- [13] R. Amer, W. Saad, B. Galkin, and N. Marchetti, "Performance analysis of mobile cellular-connected drones under practical antenna configurations," in *Proc. IEEE Int. Conf. Commun. (ICC)*, Jun. 2020, pp. 1–7.
- [14] J.-M. Kelif, M. Coupechoux, and M. Mansanarez, "A 3D beamforming analytical model for 5G wireless networks," in *Proc. 14th Int. Symp. Modeling Optim. Mobile, Ad Hoc, Wireless Netw. (WiOpt)*, May 2016, pp. 1–8.
- [15] X. Wang and M. C. Gursoy, "Coverage analysis for energy-harvesting UAV-assisted mmWave cellular networks," *IEEE J. Sel. Areas Commun.*, vol. 37, no. 12, pp. 2832–2850, Dec. 2019.
- [16] Z. Su, K. Klionovski, H. Liao, Y. Chen, A. Z. Elsherbeni, and A. Shamim, "Antenna-on-package design: Achieving near-isotropic radiation pattern and wide CP coverage simultaneously," *IEEE Trans. Antennas Propag.*, vol. 69, no. 7, pp. 3740–3749, Jul. 2021.
- [17] V. V. Chetlur and H. S. Dhillon, "Downlink coverage analysis for a finite 3-D wireless network of unmanned aerial vehicles," *IEEE Trans. Commun.*, vol. 65, no. 10, pp. 4543–4558, Jul. 2017.
- [18] A. M. Hayajneh, S. A. R. Zaidi, D. C. McLernon, M. Di Renzo, and M. Ghogho, "Performance analysis of UAV enabled disaster recovery networks: A stochastic geometric framework based on cluster processes," *IEEE Access*, vol. 6, pp. 26215–26230, 2018.
- [19] M. A. Ouamri, "Coverage and rate analysis for 5G-heterogeneous network: β -Ginibre point process," *IET Commun.*, vol. 14, no. 22, pp. 4048–4056, Dec. 2021.
- [20] M. Baianifar, S. M. Razavizadeh, S. Khavari-Moghaddam, and T. Svensson, "Effect of users height distribution on the coverage of mmWave cellular networks with 3D beamforming," *IEEE Access*, vol. 7, pp. 68091–68105, 2019.
- [21] A. A. Khuwaja, Y. Zhu, G. Zheng, Y. Chen, and W. Liu, "Performance analysis of hybrid UAV networks for probabilistic content caching," *IEEE Syst. J.*, vol. 15, no. 3, pp. 4013–4024, Sep. 2021.
- [22] K. Hosseini, W. Yu, and R. S. Adve, "Large-scale MIMO versus network MIMO for multicell interference mitigation," *IEEE J. Sel. Topics Signal Process.*, vol. 8, no. 5, pp. 930–941, Oct. 2014.
- [23] M. Alzenad and H. Yanikomeroglu, "Coverage and rate analysis for vertical heterogeneous networks (VHetNets)," *IEEE Trans. Wireless Commun.*, vol. 18, no. 12, pp. 5643–5657, Dec. 2019.
- [24] H. Alzer, "On some inequalities for the incomplete gamma function," *Math. Comput.*, vol. 66, no. 218, pp. 771–778, Apr. 1997.
- [25] (2021). *Information Technology Laboratory*. [Online]. Available: <https://www.itl.nist.gov/div898/handbook/eda/section3/eda366b.htm>
- [26] M. Cheng, J.-B. Wang, Y. Wu, X.-G. Xia, K.-K. Wong, and M. Lin, "Coverage analysis for millimeter wave cellular networks with imperfect beam alignment," *IEEE Trans. Veh. Technol.*, vol. 67, no. 9, pp. 8302–8314, Sep. 2018.
- [27] J. G. Andrews, F. Baccelli, and R. K. Ganti, "A tractable approach to coverage and rate in cellular networks," *IEEE Trans. Commun.*, vol. 59, no. 11, pp. 3122–3134, Nov. 2011.



MOHAMED AMINE OUAMRI received the M.Sc. degree from the University of Bejaia, Algeria, in 2014, and the Ph.D. degree, in 2017. From 2014 to 2015, he worked with OTA Telecom as an Engineer. He realized a Scholarship with Politehnica University Timisoara, Romania. He spent six month as a Visiting Scholar with the Université de Bretagne Occidentale, France. He is currently an Associate Professor with the University of Tizi Ouzou, Algeria. He is currently

a Research Member of the Laboratoire d'Informatique Medicale (LIMED). His research interests include wireless communication, UAV communication, D2D, satellite networks, stochastic geometry, and MIMO systems.

MOHAMMED S. ALZAIDI received the B.Sc. degree in electrical engineering from Umm Al-Qura University, Makkah, Saudi Arabia, in 2007, the M.Eng. and Ph.D. degrees in electrical engineering from the Stevens Institute of Technology, Hoboken, NJ, USA, in 2014 and 2019, respectively. He is currently an Assistant Professor with the Department of Electrical Engineering, Faculty of Engineering, Taif University, Saudi Arabia, where he is also the Vice Dean of the Deanship of Scientific Research. His research interests include nano molecular communications, wireless communications, signal processing, digital techniques, machine learning, and deep learning.



RABINDRA NATH SHAW (Senior Member, IEEE) worked as a University Examination Coordinator, a MOOCs Coordinator, a University Conference Coordinator and In Charge. As a COE PE&CEI, he has more than 11 years of teaching experience in leading institutes, such as the Motilal Nehru National Institute of Technology, Allahabad, India, Jadavpur University, and others in UG and PG level. He is currently holding the position of Faculty In-Charge International Affairs and Collaborations at Galgotias University, India (Based on document published on April 2021).

MOHAMED AZNI received the Ingénieur d'état degree in electrical engineering and the magister degree in electronics systems engineering from the Institute of Electrical and Electronics Engineering (INELEC), Boumerdes, Algeria, in 1990 and 1994, respectively, and the Ph.D. degree in electrical engineering from the University of Bejaia, Algeria, in 2010. In 1994, he joined the Electrical Engineering Department, University of Bejaia. Since then, he has been involved in many research projects. He is currently an Assistant Professor with the University of Bejaia. His research interests include signal processing and source and channel coding in wireless mobile networks and computer systems. He is currently with the LIMED Laboratory, where his research interests focus on interference management in LTE-Advanced networks and on wireless sensor networks.



SHERIF S. M. GHONEIM (Senior Member, IEEE) received the B.Sc. and M.Sc. degrees from the Faculty of Engineering, Shoubra, Zagazig University, Egypt, in 1994 and 2000, respectively, and the Ph.D. degree in electrical power and machines from the Faculty of Engineering, Cairo University, in 2008. Since 1996, he has been teaching with the Faculty of Industrial Education, Suez Canal University, Egypt. From the end of 2005 to the end of 2007, he was a Guest Researcher with the Institute of Energy Transport and Storage (ETS), University of Duisburg–Essen, Germany. After that, he joined Taif University as an Associate Professor with the Electrical Engineering Department, Faculty of Engineering. His research interests include grounding systems, dissolved gas analysis, breakdown in SF₆ gas, and AI technique applications.



DINA ALKAMA received the B.Sc. and M.Sc. degrees from the University of Bejaia, Algeria, in 2018 and 2020, respectively, where she is currently pursuing the Ph.D. degree. She is a Research Member of the Laboratoire d'Informatique Medicale (LIMED). Her research interests include resource allocation, UAV communication, wireless network analysis, and stochastic geometry.